Brazilian Journal
of Chemical
Engineering

ISSN 0104-6632
Printed in Brazil
www.abeq.org.br/bjche

Vol. 32, No. 03, pp. 757 - 765, July - September, 2015
dx.doi.org/10.1590/0104-6632.20150323s00003269

EFFECTS OF SINTERING TEMPERATURE ON THE PERFORMANCE OF $SrSc_{0.1}Co_{0.9}O_{3-\delta}$ OXYGEN SEMIPERMEABLE MEMBRANE

P. Zeng*, K. Wang, R. L. Falkenstein-Smith and J. Ahn

Department of Mechanical and Aerospace Engineering, Syracuse University, Syracuse, NY 13244, USA.
Phone +1 315-443-2946
E-mail: pizeng@syr.edu

(Submitted: February 6, 2014 ; Revised: November 3, 2014 ; Accepted: November 30, 2014)

Abstract - Our study investigates the influence of sintering temperature on the microstructure (grain size distribution, grain boundary length), electrical conductivity, and oxygen permeation properties of permeation membranes. For this purpose, $SrSc_{0.1}Co_{0.9}O_{3-\delta}$ samples with different microstructures were prepared by varying the sintering temperature from 1100 to 1250 °C. The average grain sizes were gradually increased, thus the grain boundary lengths decreased with increased sintering temperatures. The influence of the ceramic microstructure on total electrical conductivity was found to be negligible. The oxygen transport properties of the samples were characterized by permeation measurements as a function of temperature in an air/helium oxygen partial pressure gradient. The decrease of the sintering temperature, meaning a decrease of grain size and thus the increase of grain boundary length, leads to an enhanced oxygen permeation flux and a reduced activation energy. This implies that oxygen exchange and transport in the $SrSc_{0.1}Co_{0.9}O_{3-\delta}$ membranes occur more rapidly along grain boundaries than in the grain bulk.
Keywords: Oxygen permeation membrane; Perovskite; Grain size; Sintering temperature; Strontium cobalt oxide.

INTRODUCTION

Due to their intrinsic mixed conductivity, mixed ionic-electronic conductors (MIECs) with a perovskite structure are of great interest for many industrial processes in which a constant supply, or removal of, oxygen to or from gas mixtures is required (Burggraaf, 1996). Main applications include the cathode for solid oxide fuel cells (SOFCs), ultra-pure oxygen production, and hollow fiber membrane reactors for the partial oxidation of hydrocarbons to value-added products (Shao and Haile, 2004; Wang *et al*., 2005; Cheng *et al*., 2003; Zhu *et al*., 2005; Wei *et al*., 2007). Almost infinite permselectivity and remarkably high oxygen fluxes are two major advantages of these perovskite membranes (Burggraaf, 1996).

The main reason for the various applications of perovskite materials in oxygen production, or SOFCs, is their oxygen transport properties (Burggraaf, 1996; Mercle *et al*., 2004; Hamel *et al*., 2006) which are significantly influenced by differences in the microstructure of the material (i.e., grain size and homogeneousness, grain boundary distribution, and boundary composition). Recently, several studies were carried out by different groups to elucidate its importance and to address the dependence of the oxygen permeation on the microstructure (Diethelm *et al*., 2005; Zhang *et al*., 1999; Etchegoyen *et al*., 2006; Kim *et al*., 2000; Kharton *et al*., 2000; Kharton *et al*., 2001; Kharton *et al*., 2002; Arnold *et al*., 2008; Wang *et al*., 2005; Zeng *et al*., 2007; Shaula *et al*., 2005). Different perovskite systems were studied in many of these reports; however, no clear trend was visible relative to whether the transport along grain boundaries displays a barrier, or acts as a pathway for fast oxygen transport. Diethelm *et al*. (2005) found

*To whom correspondence should be addressed

for $La_{0.5}Sr_{0.5}FeO_{3-\delta}$ that the larger the obtained grains, and thus the fewer the grain boundaries, the smaller the observed oxygen permeation performance. Similar findings were reported for $SrCo_{0.8}Fe_{0.2}O_{3-\delta}$ membranes by Zhang *et al*. (1999). They observed that increasing the grain size by increasing the sintering temperature resulted in a considerable decrease in the oxygen permeation flux. Again, $La_{0.6}Sr_{0.4}Fe_{0.9}Ga_{0.1}O_{3-\delta}$ was reported by Etchegoyen *et al*. (2006) that exhibited lower oxygen permeability when the grain size of the membrane was larger. Contrary to the above findings, for the ceramics $LaCoO_{3-\delta}$, $La_{0.3}Sr_{0.7}CoO_{3-\delta}$, $La_{0.6}Sr_{0.4}Co_{0.2}Fe_{0.8}O_{3-\delta}$, $Ba_{0.5}Sr_{0.5}Co_{0.8}Fe_{0.2}O_{3-\delta}$ and $CaTi_{0.8}Fe_{0.2}O_{3-\delta}$, the increase of grain size leads to an enhanced oxygen permeation (Kharton *et al*., 2000; Kharton *et al*., 2001; Kharton *et al*., 2002; Arnold *et al*., 2008; Wang *et al*., 2005; Zeng *et al*., 2007; Shaula *et al*., 2005). Determining how microstructure influences the permeation fluxes of these mixed conducting ceramic membranes is complicated. Both the preparation procedures of the ceramic powder and the final membrane-sintering program may have significant effects on microstructure and, consequently, they will influence the oxygen permeation behavior of the resulting membranes.

In order to develop a membrane exhibiting high oxygen flux, better mechanical strength and good phase stability in a reducing atmosphere, extensive studies have been conducted in more than 20 laboratories worldwide (Teraoka *et al*., 1985; Teraoka *et al*., 1988; Diethelm *et al*., 2003 Yan *et al*., 2010; Wang *et al*., 2005; Kim *et al*., 1997; Ishihara *et al*., 2000; Schiestel *et al*., 2005; Liu *et al*., 2005; Li *et al*., 2006; Tan *et al*., 2005). Among the MIECs, $Ba_{0.5}Sr_{0.5}Co_{0.8}Fe_{0.2}O_{3-\delta}$ (BSCF) is considered to be one of the most promising materials because its membranes show high oxygen permeation fluxes and excellent cathode performance for SOFCs (Shao and Haile, 2004; Shao *et al*., 2000; McIntosh *et al*., 2006). Recently, Zeng *et al*. (2008, 2009) developed and reported a new perovskite system $SrSc_xCo_{1-x}O_{3-\delta}$ (SSCx), which also exhibits excellent cathode performance and remarkably high oxygen fluxes. Within these SSCx perovskites, $SrSc_{0.1}Co_{0.9}O_{3-\delta}$ (SSC) shows even better cathode performance and oxygen permeability than those of BSCF. Consequently, SSC is of special interest and its microstructure and oxygen permeation performance were investigated in the present study. In this paper, we present a detailed investigation of the significant effects of sintering temperature on the microstructure (i.e., grain size and grain boundary) and the oxygen permeation behavior of the $SrSc_{0.1}Co_{0.9}O_{3-\delta}$ membrane with the powder synthesized by the EDTA-citrate complexing sol-gel method.

MATERIAL AND METHODS

$SrSc_{0.1}Co_{0.9}O_{3-\delta}$ (SSC) oxide was synthesized by a combined EDTA-citrate complexing sol-gel process. $Sr(NO_3)_2$, $Co(NO_3)_2.xH_2O$, and Sc_2O_3 (all in A.R. grade) were selected as the raw materials for the metal-ion sources. Sc_2O_3 powder was first dissolved in HNO_3 solution at 90 °C under stirring. The as-obtained $Sc(NO_3)_3$ solution and $Sr(NO_3)_2$ and $Co(NO_3)_2$ were mixed with deionized water to create a mixed solution under stirring. EDTA acid powder was dissolved in $NH_3.H_2O$ solution, which was then added to the mixed solution, followed by the addition of a citric acid crystal. $NH_3.H_2O$ was used to maintain the pH value of the system at around 6. Under stirring and gentle heating at 90 °C, a clear pink solution was obtained. A clear sticky gel was finally obtained upon evaporating the water. The gel was pre-treated at 250 °C for primary decomposition and to facilitate the formation of a gray solid precursor, which was then fired at various temperatures in air for 5 h to result in the final product of SSC. The 900 °C calcined powder was pressed into disk-shaped green membranes with a diameter of 15 mm, which were then sintered, respectively, into dense membranes at 1100, 1150, 1200, and 1250 °C for 5 h under stagnant air. The sintered membranes had a diameter of 12-13 mm and thickness of 0.3 mm.

The phase structure of the samples was investigated using a Bruker D8 Advance diffractometer with Cu Kα radiation. The experimental diffraction patterns were collected at room temperature by step scanning in the range of $10^o \leq 2\theta \leq 90^o$.

The electrical conductivity was measured by the four-probe D. C. method on sintered bars under air upon cooling from 900 °C to 300 °C, lowering 10 °C per step. Silver paste was painted on the square cross sectional edges of the sample, or along the rectangular edges (separated by a distance L), to form current and voltage electrodes. Four silver wires were used in total with two as current contacts and the other two as the voltage contacts. The four silver wires were attached to the electrodes using silver paste. The sample was placed in a vertical split tube furnace. A constant current was applied to the two current wires and the voltage response on the two voltage wires were recorded using a Keithley 2420 sourcemeter.

The morphological features of the prepared membranes were examined using Environmental Scanning Microscopy (ESEM, QUANTA-2000). Based on these SEM pictures, the grain size distribution was statistically calculated by the manual measurement of the sizes of individual grains.

Permeation properties of the membranes were investigated using a high-temperature oxygen permea-

tion cell. Silver paste was used as the sealant to fix the membrane disk onto a dense quartz tube. An effective surface area of around 0.61 cm^2 was exposed for the permeation study. The sidewall of the membrane disk was also covered with silver paste to avoid radial contributions to the oxygen permeation flux. Helium was used as the sweep gas to carry the permeated oxygen to a SRI 8610C gas chromatograph equipped with a 5 Å molecular sieve capillary column for in-situ gas composition analysis. Helium also acted as the diluted gas to create the oxygen partial pressure gradient across the membrane. The test temperature was measured by a thermocouple inserted in the quartz tube at the fed gas side with an accuracy of ±1 °C. All experiments were conducted in the temperature range of 775-900 °C. The samples were first heated up to 900 °C and kept at this temperature until a steady state was reached (i.e., oxygen concentration varied less than 1%). The temperature was then dropped to the next measurement point. The oxygen permeation flux at each temperature was monitored periodically and recorded when the steady state was reached. The reported oxygen permeation fluxes are based on the steady-state values.

RESULTS AND DISCUSSION

Figure 1 shows the room-temperature X-ray diffraction (XRD) patterns of SSC calcined at 1100-1250 °C for 5 h under air. All patterns can be indexed based on a cubic symmetry. Also Zeng *et al*. (2008, 2009) have reported in previous studies that even the SSC powder calcined at a lower temperature (900 °C) shows a structure of cubic perovskite.

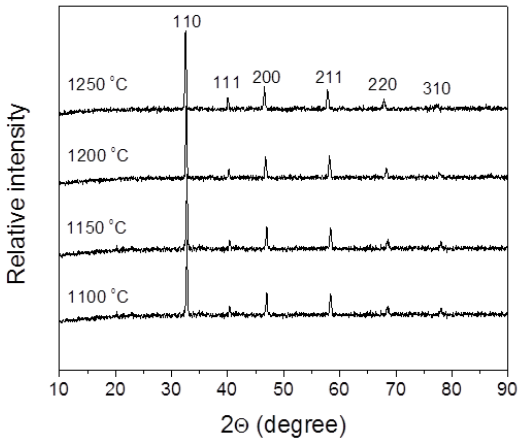

Figure 1: Room-temperature X-ray diffraction patterns of SSC calcined at 1100-1250 °C for 5 h under air.

Thus, our findings suggest that no phase transition occurred from lower to higher temperatures during the calcination or sintering process of the SSC powder precursors synthesized by the current EDTA-citrate technique. This suggests that the sintering temperature has a negligible effect on the phase structure of the current SSC membranes. The lattice parameters of all four samples were determined based on the XRD patterns and were included in Table 1. It is apparent that the lattice constant increased slightly with the increase of sintering temperature. Since both Sr^{2+} and Sc^{3+} have a fixed valence and radii of 1.44 Å and 0.745 Å, respectively, the lattice constant increase could be ascribed to the ionic radius change of cobalt ions which are Co^{3+}, 0.545 Å (LS), 0.61 Å (HS), and Co^{4+}, 0.53 Å (Dronskowski *et al*., 2005). Further, the cobalt ion was prone to adopt a high spin state at higher sintering temperatures.

Table 1: The lattice constants of the SSC samples sintered at different temperatures.

T (°C)	Symmetry	D (Å)	V ($Å^3$)
1100	Pm3m	3.8856	58.6643
1150	Pm3m	3.8894	58.8366
1200	Pm3m	3.8951	59.0956
1250	Pm3m	3.8990	59.2733

The membrane morphologies sintered at different temperatures were observed by SEM. The corresponding microstructure and grain size distribution of the various SSC membrane samples prepared at different conditions are shown in Figure 2. Obviously, the sintering temperature has a significant effect on the grain growth or size distribution of the resultant membranes. All samples displayed similar polyhedral shaped grain, while the size increased steadily with the increase of sintering temperature. The grain size distribution of the sintered membranes at various temperatures is further illustrated in Figure 3. The membrane sintered at 1100 °C had a size range of 4-40 μm with a dominant (> 90%) grain size range of 8-28 μm. When the sintering temperature was increased to 1150 °C, the grain enlarged to a range of 6-58 μm, with most of the grain within the range of 12-36 μm. The further increase of the sintering temperature to 1200 °C led to the enhancement of grain size to the range of 8-61 μm, with the majority of the grain within the range of 15-50 μm. The grain size of membranes sintered at 1250 °C spans from 16-129 μm, with the majority within the range of 30-75 μm. A substantial grain growth with the increase of the sintering temperature was also observed for other ceramics like $LaCoO_{3-\delta}$, $SrCo_{0.8}Fe_{0.2}O_{3-\delta}$ and

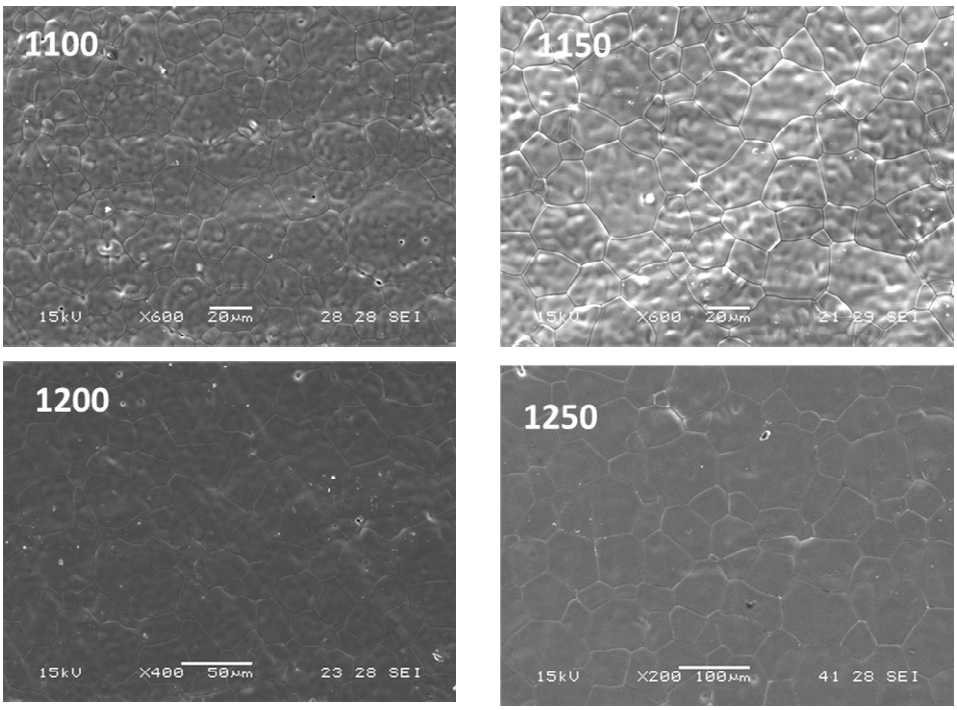

Figure 2: SEM microstructures of the various SSC membranes sintered at 1100-1250 °C for 5 h under air.

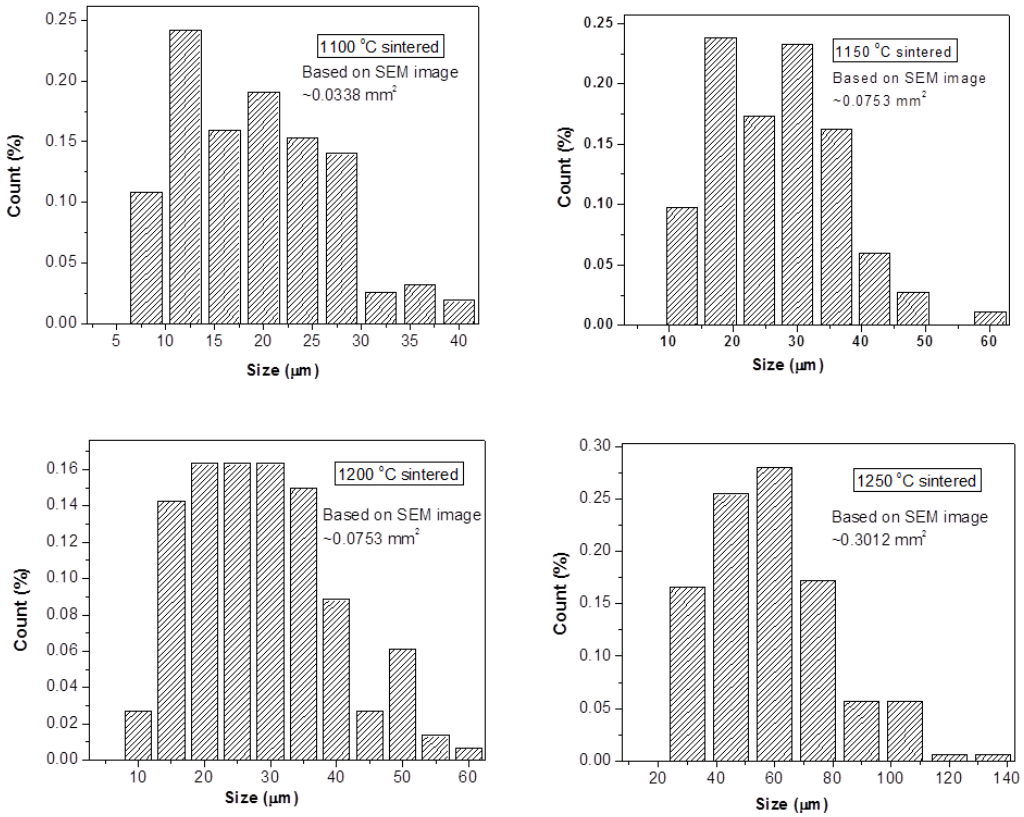

Figure 3: The temperature dependence of the grain size distribution of the membranes sintered at 1100-1250 °C.

$Ba_{0.5}Sr_{0.5}Co_{0.8}Fe_{0.2}O_{3-\delta}$ membranes (Zhang *et al*., 1999; Kharton *et al*., 2001; Wang *et al*., 2005). The grain size growth decreased the Grain Boundary Length (GBL) of the sintered ceramics. For instance, the relative GBLs of the SSC membranes sintered at 1100, 1150, 1200, and 1250 °C for 5 h are 3.0, 2.27, 1.96 and 1.0, respectively. The GBL calculation was based on the SEM results given that the grain geometry is cubic in shape. The measurement of grain size and the calculation of GBL based on the hypothesis that grain geometry is cubic in shape were previously reported in the literature (Diethelm *et al*., 2005; Zhang *et al*., 1999; Zeng *et al*., 2007). The GBL was estimated from half of the perimeter of the grains per surface area. In this study, 185, 157, 147, and 156 grains of membranes sintered at 1100, 1150, 1200, and 1250 °C for 5 h, respectively, were selected to calculate the GBLs.

The electrical conductivity of different membranes was measured by the 4-probe DC method under air, and the results are shown in Figure 4. All samples sintered at different temperatures displayed a similar trend in the change of electrical conductivities, with an initial increment, then a maximum to a subsequent decrease when the operating temperature increased from 300 to 900 °C. For a doped perovskite oxide, the electrical neutrality is compensated by the valence change of B site metal ions at low temperature. However, at a certain high temperature satisfying the formation energy of oxygen vacancies, the electrical neutrality is sustained by the formation of oxygen vacancies, and this turning temperature exhibits the peak electrical conductivity. The electronic conductivity is only associated with the valence change of B site ions, so the electrical conductivity increases with test temperatures lower than the turning temperature. However, above the turning temperature, more and more oxygen vacancies are formed, meaning less and less valence change of B site ions, resulting in the gradual reduction of the total electrical conductivity. It can be seen that the corresponding temperature of peak electrical conductivity decreases mildly with the increase of sintering temperature. This may be due to the decrease in formation energy of oxygen vacancies in samples sintered at higher temperature (Ganduglia-Pirovano *et al*., 2007). In addition, the increase of the sintering temperature from 1100 to 1250 °C resulted in a slight increase in the electrical conductivity. For example, the maximum values were 119, 129, 135 and 137 $S.cm^{-1}$ for the bars sintered at 1100, 1150, 1200 and 1250 °C, respectively. Since it is well known that the ionic conductivity σ_{ion} of mixed ionic-electronic conductors (MIECs) is typically smaller than 1 $S.cm^{-1}$, which is significantly smaller than the electronic conductivity σ_e, it could be deduced that the differences in total electrical conductivity σ_{total} between samples sintered at different temperatures are mainly due to the increases in electronic conductivity. Therefore, the slight increase of electrical conductivity (predominantly electronic) with the increase of sintering temperature, or decrease of grain boundary length, suggests that the grain boundary acts as a barrier for electron transport. This finding agrees with Maier *et al*.'s reports regarding the electrical blocking effect of the grain boundaries in doped cerium dioxide and acceptor-doped $SrTiO_3$ (Göbel *et al*., 2012; Guo *et al*., 2002). According to the report of Göbel *et al*. (2012; 2002), the following three causes can be considered to be the origin of this behavior: (i) the presence of insulating layers at the boundaries (owing to segregations of impurities); (ii) a change of the electron mobility (e.g., due to strain or related structural effects) and (iii) an increase of negatively charged point defects in the GB core; this is a reasonable hypothesis because it has been pointed out that a space charge situation with a positive space charge potential was the reason for an opposite case in which the grain boundary showed higher electrical conductivity (Gregori *et al*., 2011).

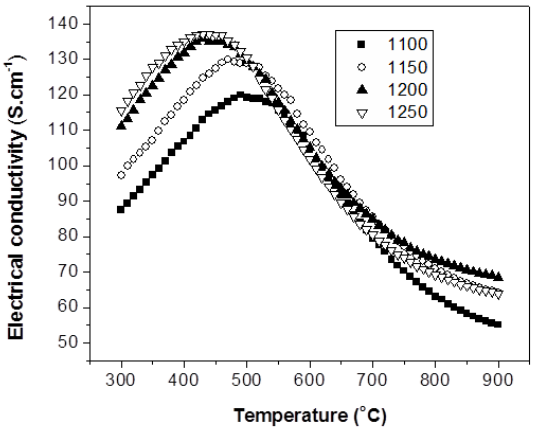

Figure 4: The electrical conductivity of the SSC membranes sintered at different temperatures.

According to the fact that significant decreases of GBLs only resulted in low increases of the electrical conductivity, we may deduce that the blocking effect of the grain boundary on the electron transport is very moderate and could even be neglected. Kharton *et al*. (2000) reported similar results for $LaCoO_{3-\delta}$ membranes, in which the influence of the ceramic microstructure on total electrical conductivity of $LaCoO_{3-\delta}$ ceramics was negligible. However, a very different phenomenon was observed for $La_{0.6}Sr_{0.4}Co_{0.2}Fe_{0.8}O_{3-\delta}$ (LSCF) by Garcia-Belmonte *et al*. (1998), who found that increasing the grain size significantly

enhanced the electrical conductivity of LSCF. Therefore, this suggests that the effect of microstructure on the conductivity is also dependent on the composition of the individual membrane material.

Figure 5 depicts the dependence of the oxygen permeability of SSC membranes on the test temperatures and membrane sintering temperatures. All of the oxygen fluxes included in Figure 5 were obtained at the constant helium sweep rate of 100 mL.min^{-1}. The oxygen permeation fluxes of all the samples clearly increase with the increase of test temperatures from 775 to 900 °C. For example, the SSC membrane sintered at 1100 °C exhibits an oxygen permeation flux of only 1.36 mL.cm^{-2}.min^{-1} at 775 °C, but a much higher flux of 3.86 mL.cm^{-2}.min^{-1} at 900 °C. Zeng *et al*. (2009) reported that a 1100 °C sintered SSC membrane with a thickness of 0.76 mm could permeate 3.2 mL oxygen per unit centimeter per minute. The membranes tested in this study are much thinner (0.3 mm) than theirs, so it is reasonable that the membrane exhibits a higher oxygen permeability of 3.86 mL.cm^{-2}.min^{-1} under the same test condition. Thus, under identical chemical activity gradients, the effective permeation rate should increase with the reciprocal of the membrane thickness. It was also reported (Zeng *et al*., 2009) that the oxygen permeation process in the 0.76 mm thick membrane was rate-limited by the relatively slower membrane gas-solid surface exchange rate (compared to the faster membrane bulk diffusion rate). Since the current membrane has a much thinner thickness of 0.3 mm, the membrane bulk diffusion rate must be much faster than that in the thicker one, which means tha the slower membrane gas-solid surface exchange process should still be the rate-limiting step for oxygen permeation in the 0.3 mm membrane.

Moreover, the oxygen permeability gradually decreases with the increase of membrane sintering temperature, and thus the grain size. For example, oxygen permeation fluxes of 3.86, 3.46, 3.18, and 2.95 mL.cm^{-2}.min^{-1} were reached for the membranes sintered at 1100, 1150, 1200 and 1250 °C, respectively, at the same test temperature of 900 °C. Figure 6 correlates the normalized GBLs of the different membranes with the oxygen fluxes measured under the same operating temperature of 900 °C. Figure 6 strongly suggests that SSC membranes with larger GBL sintered at lower temperatures possess higher oxygen permeation fluxes. For example, the corresponding oxygen fluxes through SSC membranes with relative GBLs of 3.0 and 1.0 are 3.86 and 2.95 mL.cm^{-2}.min^{-1}, respectively. Thus, this suggests that the grain boundary that has higher defect concentrations and/or higher defect jump rates than in the grain bulk acts as a faster pathway for oxygen ion exchange and transportation. This can be further proved by the decrease of the activation energy with the decrease of sintering temperature. Figure 7 shows the Arrhenius plot for the oxygen permeation flux as a function of the inverse of the temperature. The activation energies for the oxygen permeation through the membranes sintered at 1100, 1150, 1200, and 1250 °C are calculated to be 69.0, 70.0, 72.1, and 82.1 kJ.mol^{-1}, respectively, indicating that, the lower the sintering temperature, the lower the activation energy observed under similar operating conditions.

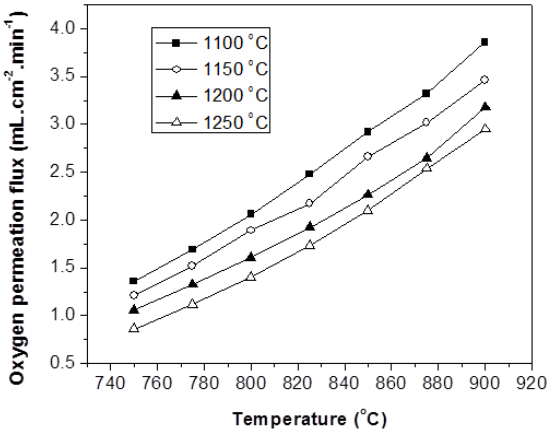

Figure 5: Temperature dependence of oxygen permeation fluxes of the SSC membranes sintered at various temperatures.

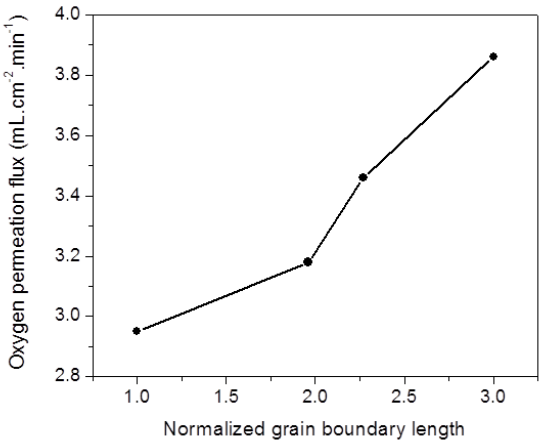

Figure 6: Dependence of oxygen fluxes permeated through various SSC samples at 900 °C on the normalized grain boundary lengths.

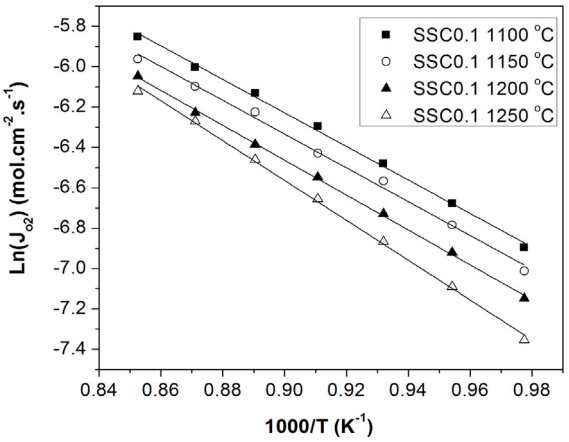

Figure 7: Arrhenius plot for the oxygen permeation flux depending on the inverse temperature.

CONCLUSION

$SrSc_{0.1}Co_{0.9}O_{3-\delta}$ samples with different microstructures were prepared by varying the sintering temperature from 1100 to 1250 °C. All samples present a cubic perovskite structure, and the lattice parameters increase moderately with the increase of sintering temperature. The microstructure of the material is affected significantly by the sintering temperature, such that the average grain size of the samples is gradually increased with the increase of sintering temperature. The influence of the ceramic microstructure on total electrical conductivity (predominantly electronic) was found to be negligible. The oxygen transport properties of the samples were characterized by permeation measurements as a function of temperature in an air/helium oxygen partial pressure gradient. The decrease of the sintering temperature, which decreases the grain size and thus increases the grain boundary length, leads to an enhanced oxygen permeation flux and reduced activation energy. This implies that oxygen exchange and transport in the $SrSc_{0.1}Co_{0.9}O_{3-\delta}$ membranes occurs more rapidly along grain boundaries than in the grain bulk. Lastly, it was deduced that the oxygen permeation process is predominantly rate-controlled by the rate of oxygen surface exchange.

REFERENCE

Arnold, M., Martynczuk, J., Efimov, K., Wang, H. and Feldhoff, A., Grain boundaries as barrier for oxygen transport in perovskite-type membranes. Journal of Membrane Science, 316, 137-144 (2008).

Burggraaf, A. J., Fundamentals of Inorganic Membrane Science and Technology. 1st Ed., Elsevier, Amsterdam (1996).

Cheng, C. S., Feng, S. J., Ran, S., Zhu, D. C., Liu, W. and Bouwmeester, H. J. M., Conversion of methane to syngas by a membrane-based oxidation reforming process. Angewandte Chemie International Edition, 42, 5196-5198 (2003).

Diethelm, S., Van Herle, J., Middleton, P. H. and Favrat, D., Oxygen permeation and stability of $La_{0.4}Ca_{0.6}Fe_{1-x}Co_xO_{3-\delta}$ (x = 0, 0.25, 0.5) membranes. Journal of Power Sources, 118, 270-275 (2003).

Diethelm, S., Van Herle, J., Sfeir, J. and Buffat, P., Correlation between oxygen transport properties and microstructure in $La_{0.5}Sr_{0.5}FeO_{3-\delta}$. Journal of the European Ceramic Society, 25, 2191-2196 (2005).

Dronskowski, R., Computational Chemistry of Solid State Materials. WILEY-VCH Verlag GmbH & Co. KGaA, Weinheim, p. 13 (2005).

Etchegoyen, G., Chartier, T. and Del-Gallo, P., Oxygen permeation in $La_{0.6}Sr_{0.4}Fe_{0.9}Ga_{0.1}O_{3-\delta}$ dense membrane: effects of surface microstructure. Journal of Solid State Electrochemistry, 10, 597-603 (2006).

Ganduglia-Pirovano, M., Hofmann, A., Sauer, J., Oxygen vacancies in transition metal and rare earth oxides: Current state of understanding and remaining challenges. Surface Science Reports, 62, 219-270 (2007).

Garcia-Belmonte, G., Bisquert, J., Fabregat, F., Kozhukharov, V. and Carda, J. B., Grain boundary role in the electrical properties of $La_{1-x}Sr_xCo_{0.8}Fe_{0.2}O_{3-\delta}$ perovskites. Solid State Ionics, 107, 203-211 (1998).

Göbel, M., Gregori, G., Maier, J., Electronically blocking grain boundaries in donor doped cerium dioxide. Solid State Ionics, 215, 45-51 (2012).

Gregori, G., Rahmati, B., Sigle, W., Aken, P., Maier, J., Electric conduction properties of boron-doped ceria. Solid State Ionics, 192, 65-69 (2011).

Guo, X., Fleig, J., Maier, J., Determination of electronic and ionic partial conductivities of a grain boundary: Method and application to acceptor-doped $SrTiO_3$. Solid State Ionics, 154-155, 563-569 (2002).

Hamel, C., Seidel-Morgenstern, A., Schiestel, T., Werth, S., Wang, H., Tablet, C. and Caro, J., Experimental and modeling study of the O_2-enrichment by perovskite fibers. AIChE Journal, 52, 3118-3125 (2006).

Ishihara, T., Yamada, T., Arikawa, H., Nishiguchi, H. and Takita Y., Mixed electronic-oxide ionic conductivity and oxygen permeating property of Fe-, Co- or Ni-doped $LaGaO_3$ perovskite oxide. Solid State Ionics, 135, 631-636 (2000).

Kharton, V. V., Fiqueiredo, F. M., Kovalevsky, A. V., Viskup, A. P., Naumovich, E. N., Yaremchenko, A. A., Bashmakov, I. A., Marques, F. M. B., Processing, microstructure and properties of $LaCoO_{3-\delta}$ ceramics. Journal of the European Ceramic Society, 21, 2301-2309 (2001).

Kharton, V. V., Kovalevsky, A. V., Yaremchenko, A. A., Fiqueiredo, F. M., Naumovich, E. N., Shaulo, A. L. and Marques, F. M. B., Surface modification of $LaSr_{0.3}Co_{0.7}O_{3-\delta}$ ceramic membranes. Journal of Membrane Science, 195, 277-287 (2002).

Kharton, V. V., Naumovich, E. N., Kovalevsky, A. V., Viskup, A. P., Figueiredo, F. M., Bashmakov, I. A. and Marques, F. M. B., Mixed electronic and ionic conductivity of $LaCo(M)O_3$ (M= Ga, Cr, Fe or Ni), IV. Effect of preparation method on oxygen transport in $LaCoO_{3-\delta}$. Solid State Ionics, 138, 135-148 (2000).

Kim, S., Wang, S., Chen, X., Yang, Y. L., Wu, N., Ignatiev, A., Jacobsen, A. J. and Abeles, B., Oxygen surface exchange in mixed ionic electronic conductors: Application to $La_{0.5}Sr_{0.5}Fe_{0.8}Ga_{0.2}O_{3-\delta}$, Journal of the Electrochemical Society, 147 (6), 2398-2406 (2000).

Kim, S., Yang, Y. L., Christoffersen, R. and Jacobson, A. J., Oxygen permeation, electrical conductivity and stability of the perovskite oxide $La_{0.2}Sr_{0.8}Cu_{0.4}Co_{0.6}O_{3-x}$. Solid State Ionics, 104, 57-65 (1997).

Li, K., Tan, X. and Liu Y., Single-step fabrication of ceramic hollow fibers for oxygen permeation. Journal of Membrane Science, 272, 1-13 (2006).

Liu, S. M. and Gavalas, G. R., Oxygen selective ceramic hollow fiber membranes. Journal of Membrane Science, 246, 103-108 (2005).

McIntosh, S., Vente, J. F., Haije, W. G., Blank, D. H. A., Bouwmeester, H. J. M., Oxygen stoichiometry and chemical expansion of $Ba_{0.5}Sr_{0.5}Co_{0.8}Fe_{0.2}O_{3-\delta}$ measured by in situ neutron diffraction. Chemistry of Materials, 18, 2187-2193 (2006).

Merkle, R., Maier, J. and Bouwmeester, H. J. M., A linear free energy relationship for gas-solid interactions: Correlation between surface rate constant and diffusion coefficient of oxygen tracer exchange for electron-rich perovskites. Angewandte Chemie International Edition, 43 5069-5073 (2004).

Schiestel, T., Kilgus, M., Peter, S., Caspary, K. J., Wang, H. H. and Caro, J., Hollow fibre perovskite membranes for oxygen separation. Journal of Membrane Science, 258, 1-4 (2005).

Shao, Z. P., Haile, S., A high-performance cathode for the next generation of solid-oxide fuel cells. Nature, 431, 170-173 (2004).

Shao, Z. P., Yang, W. S., Cong, Y., Dong, H., Tong, J. H. and Xiong, G. X., Investigation of the permeation behavior and stability of a $Ba_{0.5}Sr_{0.5}Co_{0.8}Fe_{0.2}O_{3-\delta}$ oxygen membrane. Journal of Membrane Science, 172, 177-188 (2000).

Shaula, A. L., Fuentes, R. O., Figueiredo, F. M., Kharton, V. V., Marques, F. M. B. and Frade, J. R., Grain size effects on oxygen permeation in sub micrometric $CaTi_{0.8}Fe_{0.2}O_{3-\delta}$ ceramics obtained by mechanical activation. Journal of the European Ceramic Society, 25, 2613-2616 (2005).

Tan, X., Liu, Y. and Li, K., Preparation of LSCF ceramic hollow-fiber membranes for oxygen production by a phase-inversion/sintering technique. Industrial & Engineering Chemistry Research, 44, 61-66 (2005).

Teraoka, Y., Zhang, H., Furukawa, S. and Yamazoe, N., Oxygen permeation through perovskite-type oxides. Chemistry Letters, 11, 1743-1746 (1985).

Teraoka, Y., Zhang, H., Okamoto, K. and Yamazoe, N., Mixed ionic-electronic conductivity of $La_{1-x}Sr_xCo_{1-y}Fe_yO_{3-\delta}$. Materials Research Bulletin, 23, 51-58 (1988).

Wang, H., Tablet, C., Feldhoff, A. and Caro, J., A cobalt-free oxygen-permeable membrane based on the perovskite-type oxide $Ba_{0.5}Sr_{0.5}Zn_{0.2}Fe_{0.8}O_{3-\delta}$. Advanced Materials, 17, 1785-1788 (2005).

Wang, H., Tablet, C., Feldhoff, A. and Caro, J., Investigation of phase structure, sintering, and permeability of perovskite-type $Ba_{0.5}Sr_{0.5}Co_{0.8}Fe_{0.2}O_{3-\delta}$ membranes. Journal of Membrane Science, 262, 20-26 (2005).

Wang, H., Werth, S., Schiestel, T. and Caro, J., Perovskite hollow-fibre membranes for the production of oxygen-enriched air. Angewandte Chemie International Edition, 44, 6906-6909 (2005).

Wei, B., Lu, Z., Huang, X., Liu, Z., Miao, J., Li, N., Su, W., Zhu, W., Han, W., Xiong, G. and Yang, W., Perovskite oxide as novel cathode for intermediate-temperature solid-oxide fuel cells. Journal of the American Ceramic Society, 90, 3364-3366 (2007).

Yan, L. T., Sun, W. P., Bi, L., Fang, S. M., Tao, Z. T. and Liu, W., Effect of Sm-doping on the hydrogen permeation of Ni–$La_2Ce_2O_7$ mixed protonic–electronic conductor. International Journal of Hydrogen Energy, 35, 4508-4511 (2010).

Zeng, P. Y., Ran, R., Chen, Z. H., Gu, H. X., Shao, Z. P., Costa da J. C. D. and Liu, S. M., Significant effects of sintering temperature on the performance of $La_{0.6}Sr_{0.4}Co_{0.2}Fe_{0.8}O_{3-\delta}$ oxygen selective membranes. Journal of Membrane Science, 302, 171-179 (2007).

Zeng, P. Y., Ran, R., Chen, Z. H., Zhou, W., Gu, H. X., Shao, Z. P. and Liu, S. M., Efficient stabilization of cubic perovskite $SrCoO_{3-\delta}$ by B-site low concentration scandium doping combined with sol–gel synthesis. Journal of Alloys and Compounds, 455, 465-470 (2008).

Zeng, P. Y., Ran, R., Hao, Y., Shao, Z. P. and Liu, S. M., Effects of scandium doping concentration on the properties of strontium cobalt oxide membranes. Brazilian Journal of Chemical Engineering, 26, 563-574 (2009).

Zhang, K., Yang, Y. L., Ponnusamy, D., Jacobson, A. J. and Salama, K., Effect of microstructure on oxygen permeation in $SrCo_{0.8}Fe_{0.2}O_{3-\delta}$. Journal of Materials Science, 34, 1367-1372 (1999).

Zhu, W., Han, W., Xiong, G. and Yang, W., Mixed reforming of heptane to syngas in the $Ba_{0.5}Sr_{0.5}Co_{0.8}Fe_{0.2}O_{3-\delta}$ membrane reactor. Catalysis Today, 104, 149-153 (2005).